remote sensing

MDPI

Article

Hyperspectral Leaf Area Index and Chlorophyll Retrieval over Forest and Row-Structured Vineyard Canopies

Luke A. Brown [1,2,*], Harry Morris [2,3], Andrew MacLachlan [2,4], Francesco D'Adamo [2,5], Jennifer Adams [6,7], Ernesto Lopez-Baeza [8,9], Erika Albero [8], Beatriz Martínez [8], Sergio Sánchez-Ruiz [8], Manuel Campos-Taberner [8], Antonio Lidón [10], Cristina Lull [10], Inmaculada Bautista [10], Daniel Clewley [11], Gary Llewellyn [12,13], Qiaoyun Xie [14], Fernando Camacho [15], Julio Pastor-Guzman [2,16], Rosalinda Morrone [3,17], Morven Sinclair [3], Owen Williams [2], Merryn Hunt [2,18], Andreas Hueni [6], Valentina Boccia [19], Steffen Dransfeld [19] and Jadunandan Dash [2]

1 School of Science, Engineering & Environment, University of Salford, Manchester M5 4WT, UK
2 School of Geography and Environmental Science, University of Southampton, Southampton SO17 1BJ, UK
3 Climate and Earth Observation Group, National Physical Laboratory, Teddington TW11 0LW, UK; r.morrone@stariongroup.eu (R.M.)
4 The Bartlett Centre for Advanced Spatial Analysis, University College London, London W1T 4TJ, UK
5 Centre for Ecological Research and Forestry Applications (CREAF), 08193 Barcelona, Spain
6 Department of Geography, University of Zürich, 8057 Zürich, Switzerland
7 European Commission Joint Research Centre, 21027 Ispra, Italy
8 Departament de Física de la Terra i Termodinàmica, Facultat de Física, Universitat de València, 46100 Burjassot, Spain
9 Albavalor S.L.U., Parc Científic Universitat de València, 46980 Paterna, Spain
10 Research Group in Forest Science and Technology (Re-ForeST), Research Institute of Water and Environmental Engineering (IIAMA), Universitat Politècnica de València, Camí de Vera s/n, 46022 València, Spain
11 Natural Environment Research Council Earth Observation Data Acquisition and Analysis Service (NEODASS), Plymouth Marine Laboratory, Plymouth PL1 3DH, UK
12 2Excel Geo, Sywell, Northampton NN6 0BN, UK
13 Natural Environment Research Council Airborne Research Facility (NERC ARF), British Antarctic Survey, Cambridge CB3 0ET, UK
14 Department of Civil, Environmental and Mining Engineering, University of Western Australia, Perth, WA 6009, Australia
15 Earth Observation Laboratory (EOLAB), 46980 Paterna, Spain
16 Tecnológico Nacional de México/IT Bahía de Banderas, Crucero a Punta de Mita s/n, Bahía de Banderas, Nayarit 63734, Mexico
17 Starion, 00044 Frascati, Italy
18 UK Centre for Ecology and Hydrology, Lancaster Environment Centre, Lancaster LA1 4AP, UK
19 European Space Research Institute, European Space Agency, 00044 Frascati, Italy
* Correspondence: l.a.brown4@salford.ac.uk

check for updates

Citation: Brown, L.A.; Morris, H.; MacLachlan, A.; D'Adamo, F.; Adams, J.; Lopez-Baeza, E.; Albero, E.; Martínez, B.; Sánchez-Ruiz, S.; Campos-Taberner, M.; et al. Hyperspectral Leaf Area Index and Chlorophyll Retrieval over Forest and Row-Structured Vineyard Canopies. *Remote Sens.* **2024**, *16*, 2066. https://doi.org/10.3390/rs16122066

Academic Editor: Liang Sun

Received: 12 April 2024
Revised: 14 May 2024
Accepted: 4 June 2024
Published: 7 June 2024

Abstract: As an unprecedented stream of decametric hyperspectral observations becomes available from recent and upcoming spaceborne missions, effective algorithms are required to retrieve vegetation biophysical and biochemical variables such as leaf area index (LAI) and canopy chlorophyll content (CCC). In the context of missions such as the Environmental Mapping and Analysis Program (EnMAP), Precursore Iperspettrale della Missione Applicativa (PRISMA), Copernicus Hyperspectral Imaging Mission for the Environment (CHIME), and Surface Biology Geology (SBG), several retrieval algorithms have been developed based upon the turbid medium Scattering by Arbitrarily Inclined Leaves (SAIL) radiative transfer model. Whilst well suited to cereal crops, SAIL is known to perform comparatively poorly over more heterogeneous canopies (including forests and row-structured crops). In this paper, we investigate the application of hybrid radiative transfer models, including a modified version of SAIL (rowSAIL) and the Invertible Forest Reflectance Model (INFORM), to such canopies. Unlike SAIL, which assumes a horizontally homogeneous canopy, such models partition the canopy into geometric objects, which are themselves treated as turbid media. By enabling crown transmittance, foliage clumping, and shadowing to be represented, they provide a more realistic representation of heterogeneous vegetation. Using airborne hyperspectral data to simulate EnMAP observations over vineyard and deciduous broadleaf forest sites, we demonstrate that SAIL-based

algorithms provide moderate retrieval accuracy for LAI (RMSD = 0.92–2.15, NRMSD = 40–67%, bias = −0.64–0.96) and CCC (RMSD = 0.27–1.27 g m^{-2}, NRMSD = 64–84%, bias = −0.17–0.89 g m^{-2}). The use of hybrid radiative transfer models (rowSAIL and INFORM) reduces bias in LAI (RMSD = 0.88–1.64, NRMSD = 27–64%, bias = −0.78–−0.13) and CCC (RMSD = 0.30–0.87 g m^{-2}, NRMSD = 52–73%, bias = 0.03–0.42 g m^{-2}) retrievals. Based on our results, at the canopy level, we recommend that hybrid radiative transfer models such as rowSAIL and INFORM are further adopted for hyperspectral biophysical and biochemical variable retrieval over heterogeneous vegetation.

Keywords: CCC; CHIME; EnMAP; INFORM; LAI; PRISMA; SAIL; SBG

1. Introduction

With recent and upcoming spaceborne missions such as the Environmental Mapping and Analysis Program (EnMAP) [1], Precursore Iperspettrale della Missione Applicativa (PRISMA) [2], Copernicus Hyperspectral Imaging Mission for the Environment (CHIME) [3] and Surface Biology and Geology (SBG) [4], an unprecedented stream of hyperspectral observations covering the visible, near-infrared, and shortwave-infrared regions of the electromagnetic spectrum (i.e., 400–2500 nm) is becoming available. Previously restricted to costly and infrequent airborne campaigns or tasked acquisitions from experimental spaceborne instruments such as the Compact High Resolution Imaging Spectrometer (CHRIS) and Hyperion, hyperspectral observations are now provided on a regular basis at decametric (i.e., 10–100 m) scale [1,2,5]. To exploit these observations for vegetation monitoring, accurate and effective algorithms are required to retrieve the biophysical and biochemical variables that describe vegetation conditions.

Key vegetation biophysical and biochemical variables include leaf area index (LAI), which represents half the unit surface area of leaves per unit horizontal ground area [6], and canopy chlorophyll content (CCC). CCC is determined as the product of LAI and leaf chlorophyll concentration (LCC), which itself describes the quantity of chlorophyll per unit leaf area or unit leaf mass [7]. As a measure of canopy structure, LAI defines the size of the interface between the biosphere and atmosphere, and consequently the interception of light, precipitation, and biogeochemical fluxes [8,9]. Meanwhile, CCC is a sensitive indicator of vegetation physiological status, owing to chlorophyll's crucial role in photosynthesis [10,11]. As a result, estimates of LAI and CCC are required not only for monitoring agricultural and forest condition, but also for modelling vegetation productivity, carbon exchange, and the weather and climate systems [8,9,12].

The retrieval of LAI and CCC from hyperspectral observations typically involves (i) statistical methods, or (ii) the use of coupled leaf and canopy radiative transfer models that simulate observed reflectance as a function of biophysical and biochemical properties [13,14]. The statistical approach establishes an empirical relationship between reflectance observations (or derived spectral indices) and the biophysical or biochemical variable of interest. Whilst straightforward, because globally representative in situ sampling is difficult to achieve, these relationships tend to be specific to a given site, species/vegetation type, and observation scenario, meaning they may lack generality [13,15–22]. In contrast, the radiative transfer model-based approach uses simulations to populate look-up-tables or train machine learning algorithms for retrieval, with the physical basis of the models potentially providing greater universal applicability [13,23–26].

In the context of decametric hyperspectral observations (such as those from EnMAP, PRISMA, and CHIME), several radiative transfer model-based algorithms have been developed for LAI and CCC retrieval, with a primary focus on cereal crops [27–31]. The majority of these algorithms have adopted Scattering by Arbitrarily Inclined Leaves (SAIL) [32,33] as the canopy radiative transfer model. SAIL represents the canopy as a horizontally homogeneous turbid medium, and whilst it is well suited to dense, leafy, and homogeneous canopies (such as cereal crops and grasslands), it is known to perform comparatively poorly

over more heterogeneous canopies (including forests and row-structured crops) [25,34–36]. Over such canopies, less attention to the retrieval of LAI and CCC from decametric hyperspectral observations has been paid so far.

To address the drawbacks of SAIL over forest and row-structured crop canopies, recent work on multispectral LAI and CCC retrieval has applied hybrid radiative transfer models [35,37–40]. Unlike SAIL, these models partition the canopy into geometric objects, which are themselves treated as turbid media. By enabling crown transmittance, foliage clumping, and shadowing to be represented, they provide a more realistic representation of heterogeneous vegetation [17,20,39,41,42]. Despite this improved representation, they offer a lower level of complexity than three-dimensional radiative transfer models, which require extensive parameterisation (and as a result of the ill-posed nature of the inverse problem, are challenging to invert) [20,41]. In this paper, we investigate the application of such hybrid radiative transfer models to hyperspectral observations. Using airborne hyperspectral data to simulate EnMAP observations over vineyard and deciduous broadleaf forest sites, we address the following research questions:

1. What accuracy might be expected when SAIL-based LAI and CCC retrieval algorithms are applied to decametric hyperspectral observations over two distinct types of heterogeneous canopy?
2. Are some biophysical or biochemical variables better retrieved than others?
3. To what extent can hybrid radiative transfer models improve retrieval accuracy over such environments?

Over the investigated sites, we hypothesise that (i) SAIL-based LAI and CCC retrievals will be characterised by moderate accuracy; (ii) LAI will be better retrieved than CCC; and (iii) the hybrid radiative transfer models will reduce bias when compared to SAIL-based retrievals.

2. Materials and Methods

2.1. Airborne Hyperspectral Data Acquisition

Three campaigns involving the acquisition of airborne hyperspectral data were carried out between 2017 and 2021 in Spain and the United Kingdom. The first took place over a 10 km × 10 km area of the Valencia Anchor Station, Valencian Community, Spain (39.5707°N, 1.2882°W), which is located in the Utiel-Requena plateau. It lies approximately 80 km west of Valencia, and is dominated by vineyards (*Vitis vinifera*), as well as almond (*Prunus dulcis*), olive (*Olea europaea*), and some smaller areas of shrubland and Aleppo pine (*Pinus halepensis*) [43]. Airborne hyperspectral data covering the area were acquired on 17 June 2017 by the Natural Environment Research Council (NERC) Airborne Research Facility (ARF) using the Specim AisaFENIX instrument (Specim, Oulu, Finland) [44] (Figure 1 and Table 1). Conditions during the flight were clear and dominated by direct illumination, with low humidity (<30%), high atmospheric pressure (>1018 mbar), low wind speeds (<4 m s^{-1}), and air temperatures of 32–37 °C.

Table 1. Summary of the airborne hyperspectral datasets acquired during each campaign.

Campaign	Date	Instrument	Operator	Spectral Range (nm)	FWHM (nm)	FOV (°)	Spatial Pixels	Spectral Pixels	Flight Lines	Spatial Resolution (m)
Valencia Anchor Station 2017	17 June	Specim AisaFENIX	NERC ARF	380–2500	3.5 nm (VNIR), 12 nm (SWIR)	32	384	623	21	2
Wytham Woods 2018	3 July							622	13	
Wytham Woods 2021	16 July	NASA JPL AVIRIS-NG	UZH ARES	380–2510	5 nm	36	640	480	2	3

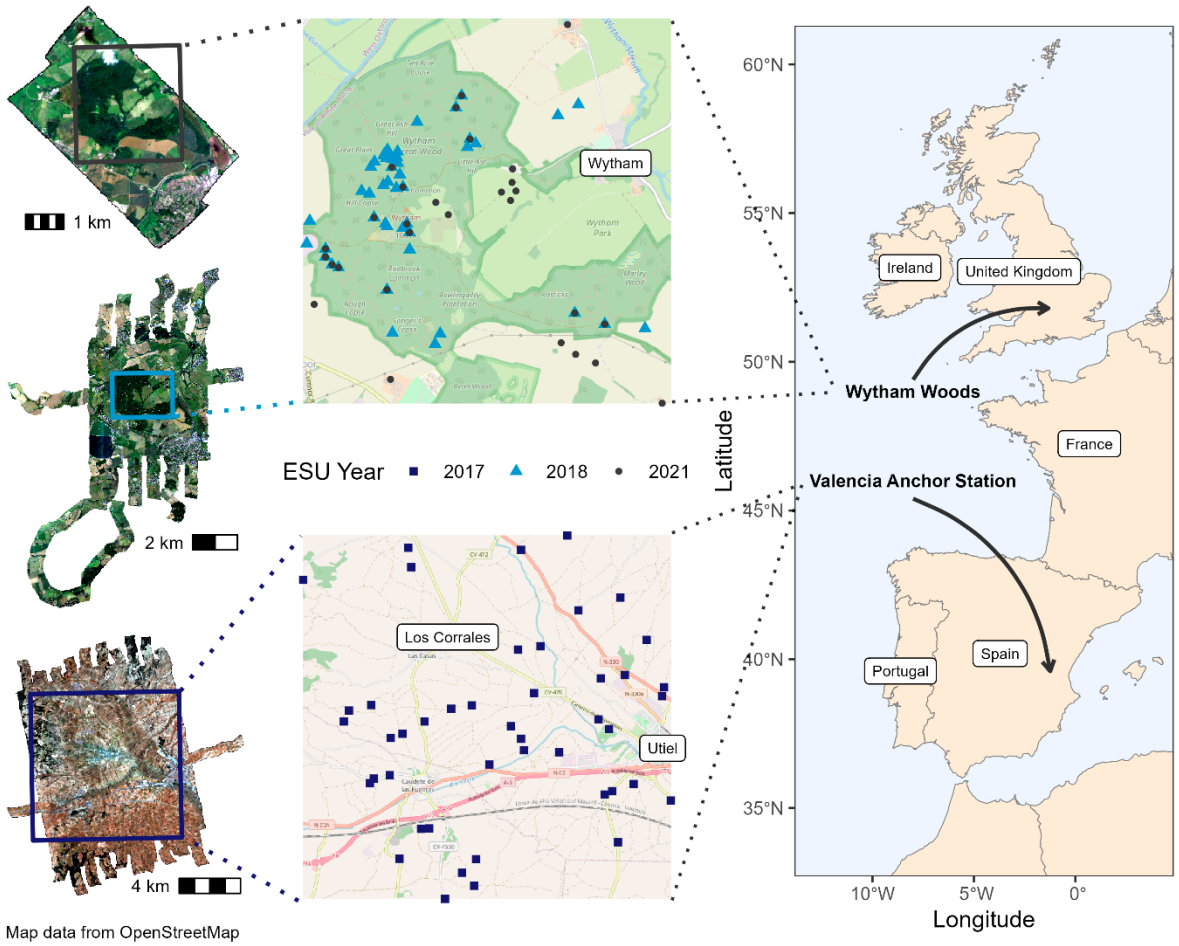

Figure 1. True colour composite airborne hyperspectral mosaics collected during the Wytham Woods 2021 (**top left**), Wytham Woods 2018 (**middle left**), and Valencia Anchor Station 2017 (**bottom left**) campaigns, in addition to the location of the elementary sampling units (ESUs) in which in situ LAI and LCC measurements were performed (**middle**), and the location of each study site (**right**).

The second and third campaigns were conducted over a 3 km × 3 km area of Wytham Woods, Oxfordshire, United Kingdom (51.7734°N, 1.3384°W), which lies approximately 5 km west of Oxford, and is characterised by ancient and seminatural woodland. The dominant species are oak (*Quercus robur*), ash (*Fraxinus excelsior*), beech (*Fagus sylvatica*), hazel (*Corylus avellana*), and sycamore (*Acer pseudoplatanus*). Airborne hyperspectral data were acquired on 3 July 2018 by NERC ARF, again using the Specim AisaFENIX, and on 17 July 2021 by the University of Zürich (UZH) Airborne Research Facility for Earth System (ARES), in this case using the Airborne Visible/Infrared Imaging Spectrometer Next Generation (AVIRIS-NG) instrument developed at the National Aeronautics and Space Administration (NASA) Jet Propulsion Laboratory (JPL) (Pasadena, CA, USA) [45] (Figure 1 and Table 1). AVIRIS-NG was deployed in 2021 in Europe as part of the mission preparation for the European Space Agency (ESA) CHIME and NASA SBG missions [46]. Conditions during both flights were clear (though with one small cloud on 17 July 2021, see Figure 1) and were characterised by low to medium humidity (26–54%), high atmospheric pressure (>1015 mbar), low wind speeds (<6 m s^{-1}), and air temperatures of 25–27 °C.

During the Valencia Anchor Station 2017 and Wytham Woods 2018 campaigns, simultaneous aerosol optical thickness (AOT) measurements were acquired with a Solar Light Company Microtops II sunphotometer (Glenside, PA, USA). In the former campaign, the hemispherical-conical reflectance factor (HCRF) of several in-scene targets (including white, grey, and black 12 m × 9 m tarpaulins and an artificial football field) was also determined

to enable the verification of the atmospheric correction approach (over a reduced spectral range due to the limitations of the available spectroradiometer) (Figure 2). These measurements were achieved using an Analytical Spectral Devices (ASD) FieldSpec 3 Visible Near-Infrared (VNIR) (Boulder, CO, USA) and Spectralon SRT-99-100 panel (Labsphere Inc., North Sutton, NH, USA). Prior to the campaigns, the Spectralon panel was cleaned and calibrated by the NERC Field Spectroscopy Facility (FSF), enabling the absolute HCRF to be calculated. For each tarpaulin, the mean of 40 measurements was determined.

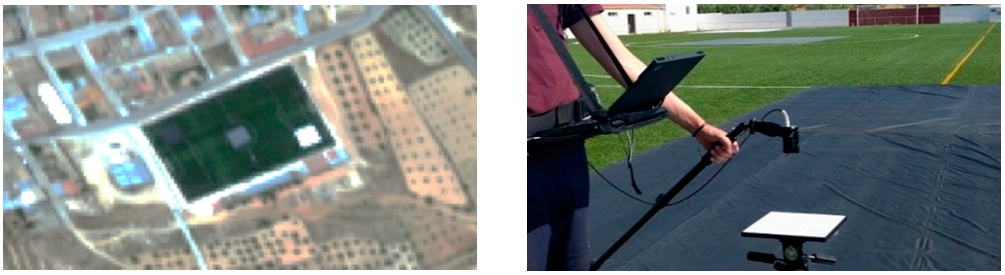

(**a**) (**b**)

Figure 2. True colour composite of airborne hyperspectral data over the in-scene targets (**a**) for which HCRF was determined using an ASD FieldSpec 3 VNIR spectroradiometer (**b**) in the Valencia Anchor Station 2017 campaign.

2.2. Airborne Hyperspectral Data Pre-Processing

Data collected by NERC ARF during the Valencia Anchor Station 2017 and Wytham Woods 2018 campaigns were delivered as individual L1B radiometrically corrected flight lines in sensor geometry, whilst data collected by UZH ARES during the Wytham Woods 2021 campaign had already been radiometrically, atmospherically and geometrically corrected prior to delivery [45,47]. The atmospheric correction of the NERC ARF datasets was performed by the NERC ARF Data Analysis Node using ATCOR-4 for the Valencia Anchor Station 2017 campaign. For the Wytham Woods 2018 campaign, the Fast Line of Sight Atmospheric Analysis of Spectral Hypercubes (FLAASH) module incorporated in the Environment for Visualising Images (ENVI) was used. Both approaches are based on the underlying MODTRAN5 radiative transfer model [48]. To verify the compatibility between ATCOR-4 and FLAASH, the flight line containing tarpaulins in the Valencia Anchor Station 2017 campaign was also processed with FLAASH, facilitating comparison (Section 3.1).

The parameterisation of ATCOR-4 and FLAASH was achieved using an atmospheric model appropriate to each site's latitude, a rural aerosol model, and visibility values derived from the AOT data collected at the time of each flight line (Section 2.1). Since the Microtops II does not measure AOT at 550 nm, it was derived by interpolating between AOT at 440 nm and 675 nm using the Angström power law. The Angström exponent was first calculated as

$$\alpha = -\frac{\ln(\tau_{440}/\tau_{675})}{\ln(440/675)} \quad (1)$$

where τ_{440} and τ_{675} are AOT values at 440 nm and 675 nm, before determining the AOT at 550 nm as

$$\tau_{550} = \tau_{440}\frac{550}{440}^{-\alpha} \quad (2)$$

AOT values were then converted to visibility (km) following [49], such that

$$V_{550} = \frac{3.912}{\tau_{550}} \quad (3)$$

Water vapour was retrieved from the imagery itself, using the water absorption feature at 1135 nm. Ground-level altitude was determined for each flight line based on the

supplied Advanced Spaceborne Thermal Emission and Reflection Radiometer (ASTER) Global Digital Elevation Model (GDEM), referenced with respect to the World Geodetic System 1984 ellipsoid.

Following atmospheric correction, to account for limb-brightening effects observed in each flight line, we carried out cross-track illumination correction according to [50], using a second-order polynomial multiplicative model fit to the mean of each column of each image. Subsequently, each flight line was geometrically corrected using the Airborne Processing Library (APL) [51], before being mosaicked in ENVI. Finally, to simulate the spectral and spatial characteristics of recent and upcoming spaceborne hyperspectral missions, each mosaic was spectrally resampled according to the measured central wavelength and full-width at half-maximum (FWHM) of the 218 bands available from EnMAP, assuming a Gaussian spectral response, before being aggregated to a 30 m spatial resolution using mean value downsampling.

2.3. Airborne Hyperspectral LAI and CCC Retrieval

To retrieve LAI and CCC from the airborne hyperspectral data, three canopy radiative transfer models were considered:

1. SAIL [32,33];
2. A modified version of SAIL, hereafter termed rowSAIL, which accounts for the structure of row-planted vegetation. As detailed in [37], the modifications in rowSAIL are equivalent to those made to the Markov Chain Canopy Reflectance Model (MCRM) under the Crop Reflectance Operational Models for Agriculture (CROMA) project, which resulted in the so-called rowMCRM model [39,42];
3. The Invertible Forest Reflectance Model (INFORM) [41,52], which accounts for the structure of forest canopies.

Whilst SAIL can be considered a turbid medium radiative transfer model, describing the canopy as a horizontally homogeneous series of randomly oriented scatterers (Figure 3a), rowSAIL and INFORM are hybrid radiative transfer models (Figure 3b,c).

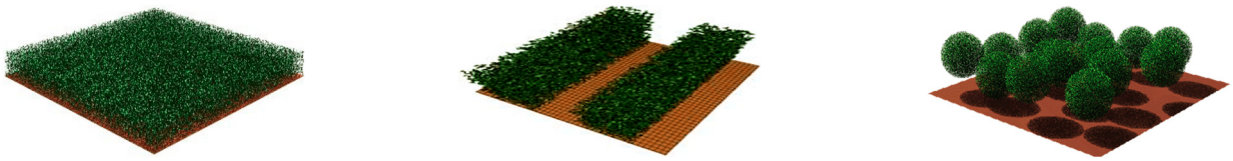

(**a**) (**b**) (**c**)

Figure 3. Graphical representation of turbid medium (**a**) and hybrid radiative transfer models representing row-structured crop (**b**) and forest (**c**) canopies, in which the canopy is represented by geometric objects that are themselves treated as turbid media. Adapted from [53–55].

The rowMCRM model that rowSAIL is based upon is detailed by [39,42], whilst a detailed description of INFORM is provided by [41,52]. Briefly, rowSAIL computes canopy reflectance as a linear mixture of canopy (as simulated by SAIL), sunlit soil, and shaded soil reflectance, weighted by the fractions of the scene covered by each, which are geometrically determined on the basis of the viewing and illumination geometry, row height, row width, row orientation, and the width of the soil strip between rows [39,42]. INFORM is an extension of the Forest Light Interaction Model (FLIM), which computes canopy reflectance as a linear mixture of crown reflectance at infinite crown depth and background reflectance, weighted by the 'crown factor' (accounting for crown transmittance and the fraction of the scene covered by crowns) and the 'ground factor' (accounting for the fraction of sunlit and shaded soil beneath and outside of tree crowns). In FLIM, crown transmittance is computed from simple exponential functions of LAI, whilst crown reflectance at infinite crown depth and background reflectance are derived from image endmembers. INFORM makes use of SAIL to determine these parameters [41,52].

In all cases, leaf optical properties were simulated by Leaf Optical Properties Spectra (PROSPECT) [56,57]. For each site, two look-up-tables were populated, each with 100,000 reflectance simulations. Input parameters were randomly drawn from fixed, uniform, or truncated Gaussian distributions (Tables 2 and 3).

Table 2. Distributions from which PROSPECT, SAIL, and rowSAIL parameters were randomly drawn to populate look-up-tables for LAI and CCC retrieval at the Valencia Anchor Station.

Model	Parameter	Minimum	Maximum	Mean	Standard Deviation
PROSPECT	Structural parameter (N)	1.62	1.62	-	-
	Chlorophyll a + b (μg cm^{-2})	30	45	35	5
	Dry matter (g cm^{-2})	0.0035	0.0035	-	-
	Equivalent water thickness (g cm^{-2})	0.025	0.025	-	-
Common to SAIL and rowSAIL	Average leaf angle (°)	45	45	-	-
	LAI	0.0	3.0	1.5	0.5
	Hotspot parameter	0.083	0.083	-	-
	Solar zenith angle (°)	22	43	-	-
	Observer zenith angle (°)	0	16	-	-
	Relative azimuth angle (°)	97	133	-	-
	Fraction of diffuse radiation	0.15	0.15	-	-
	Soil brightness coefficient	0.6	1.4	1	0.5
Specific to rowSAIL	Row height (m)	1.2	1.8	-	-
	Row width (m)	0.6	1.3	-	-
	Visible soil strip (m)	1.5	3.0	2.4	0.3
	Difference between solar azimuth angle and row direction (°)	0	126	50	43

Table 3. Distributions from which PROSPECT, SAIL, and INFORM parameters were randomly drawn to populate look-up-tables for LAI and CCC retrieval at Wytham Woods.

Model	Parameter	Minimum	Maximum	Mean	Standard Deviation
PROSPECT	Structural parameter (N)	1.5	1.7	-	-
	Chlorophyll a + b (μg cm^{-2})	0	60	30	20
	Dry matter (g cm^{-2})	0.004	0.020	-	-
	Equivalent water thickness (g cm^{-2})	0.01	0.02	-	-
Common to SAIL and INFORM	Average leaf angle (°)	55	55	-	-
	LAI	0.0	8.0	5.0	0.5
	Hotspot parameter	1.4	1.4	-	-
	Solar zenith angle (°)	30	42	-	-
	Observer zenith angle (°)	0	16	-	-
	Relative azimuth angle (°)	120	162	-	-
	Fraction of diffuse radiation	0.1	0.1	-	-
	Soil brightness coefficient	0.5	0.5	-	-
Specific to INFORM	Understory LAI	0.0	5.0	1.0	0.5
	Stem density (ha^{-1})	0	1130	-	-
	Canopy height (m)	10	20	-	-
	Crown diameter (m)	6	14	8	4

For each simulation, a soil spectrum was randomly selected from a spectral library containing 25 soils [58] and multiplied by a soil brightness coefficient. For the Valencia Anchor Station, this was restricted to a subset of 10 sandy loam soils to better reflect the characteristics of the site [37]. The two look-up-tables were constructed using SAIL and rowSAIL simulations in the case of the Valencia Anchor Station (due to the presence of row-structured crops), and SAIL and INFORM simulations in the case of Wytham

Woods (due to the presence of a forest canopy). For input parameters common to the two models in question, the same distributions were used (Tables 2 and 3). As for the airborne hyperspectral data (Section 2.2), the reflectance simulations were spectrally resampled to match the 218 bands available from EnMAP.

Retrieval was achieved by comparing observed airborne hyperspectral reflectance spectra with the simulated spectra stored in each look-up-table. To avoid noisy spectral regions dominated by water vapour absorption, bands between 1300–1500 nm and 1700–2000 nm were excluded. After atmospheric correction, we observed substantial residual noise (i.e., dropouts) between 800–1000 nm, so bands within this wavelength range were also excluded. Previous work has shown that, due to the presence of noise and measurement uncertainties, the use of the closest match may not provide the most robust retrievals [59–62]. As such, the mean LAI and CCC values associated with the 100 closest matches in terms of their root mean square difference (RMSD) over all bands was computed as the retrieved value. All bands were given equal weighting in the computation of the RMSD.

2.4. Validation of LAI and CCC Retrievals against In Situ Measurements

To facilitate the validation of the retrievals, in situ LAI and LCC measurements were conducted within several days of each flight, and were carried out within elementary sampling units (ESUs) of between 20 m × 20 m and 40 m × 40 m (Figure 1). Each ESU contained 10–20 measurement locations (Table 4). To enable the row structure of the canopy to be characterised in the Valencia Anchor Station 2017 campaign, within each ESU, measurements were conducted along transects positioned diagonally with respect to the planting direction (with LAI measurements conducted within and between rows, and LCC measurements conducted within rows only) [37]. In the Wytham Woods 2018 and 2021 campaigns, which took place under the Fiducial Reference Measurements for Vegetation (FRM4VEG) programme [63], a systematic within-ESU sampling scheme was adopted following LAI validation good practices [64].

Table 4. Summary of the in situ LAI and LCC measurements acquired during each campaign.

Campaign	Dates	Sampled ESUs		ESU Dimensions	Within-ESU Sampling Locations	Reference
		LAI	LCC			
Valencia Anchor Station 2017	14–16 June	45	40	40 m × 40 m	10–20	[37]
Wytham Woods 2018	3–5 July	47	30	20 m × 20 m	13–15	[63]
Wytham Woods 2021	20–23 July	29	29	20 m × 20 m	13–15	This study

In all cases, LAI was determined via digital hemispherical photography (DHP), using either a Nikon Coolpix 4500 and FC-E8 fisheye lens (Nikon Inc., Melville, NY, USA), Canon EOS 6D (Canon, Tokyo, Japan) and Sigma 8 mm F3.5 EX DG fisheye lens (Sigma, Kawasaki, Japan), or Canon EOS 60D and Sigma 4.5 mm F2.8 EX DC fisheye lens [37,63]. Images from the Valencia Anchor Station 2017 campaign were processed with HemiPy [65]. Those from the Wytham Woods 2018 and 2021 campaigns (which consisted of both upwards- and downwards-facing images to capture the overstory and understory) were processed with CAN-EYE [66]. LCC was determined using the Konica Minolta SPAD-502 chlorophyll meter (Konica Minolta, Inc., Tokyo, Japan), and at each sampling location, chlorophyll meter measurements were made on one to three leaves, with six replicates per leaf, yielding a total of 78–234 measurements per ESU. Relative values provided by the chlorophyll meter were converted to absolute units by means of laboratory-derived calibration functions [37,63,67,68]. ESU-level CCC was determined as the product of LAI and mean LCC.

Validation of the hyperspectral retrievals was achieved by comparison with in situ LAI and CCC. Overall agreement was quantified in terms of the coefficient of determination

(r^2), RMSD, normalised RMSD (NRMSD) (which was computed by dividing the RMSD by the mean of the in situ values), and bias (which was computed as the mean difference).

3. Results

3.1. Consistency of Atmospheric Correction Approaches

When assessed over the in-scene targets in the Valencia Anchor Station 2017 campaign, both ATCOR-4 and FLAASH provided similar reflectance spectra (Figure 4). Both demonstrated good agreement with in situ measurements of HCRF between 350–1050 nm (RMSD $\leq$ 0.07, NRMSD $\leq$ 23%, bias $\leq$ 0.02), with the exception of FLAASH over the black tarpaulin (NRMSD = 55%) (Table 5). Compared to the in situ measurements, for unsaturated wavelengths, both ATCOR-4 and FLAASH slightly underestimated reflectance over the white tarpaulin (bias = −0.03) and artificial football field (bias = −0.01), but provided unbiased or slightly overestimated reflectance values over the black tarpaulin (bias = 0.00–0.02) and grey tarpaulin (bias = 0.01) (Table 5). Despite FLAASH producing slightly nosier spectra (Figure 4), its good agreement with ATCOR-4 confirms its compatibility, indicating that differences between the atmospheric correction approach adopted in each campaign should not substantially influence our results.

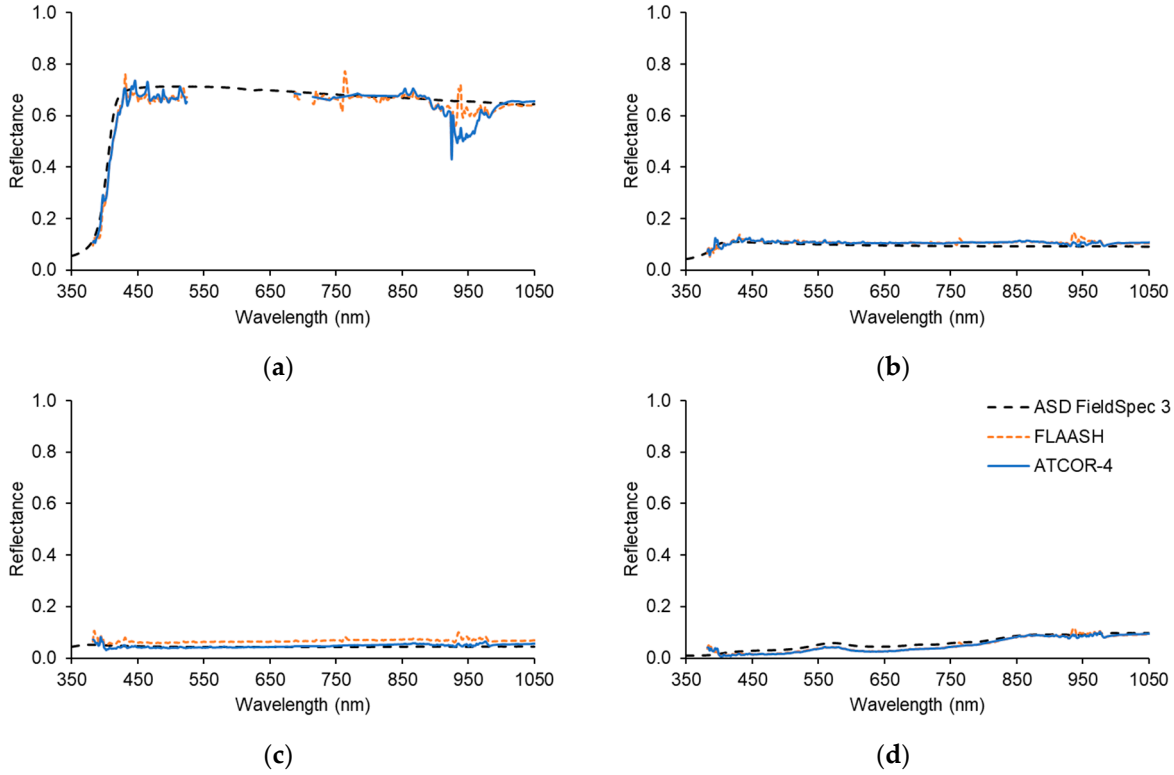

Figure 4. Reflectance of the white tarpaulin (**a**), grey tarpaulin (**b**), black tarpaulin (**c**), and artificial football field (**d**) between 350–1050 nm in the Valencia Anchor Station 2017 campaign, as determined from the airborne hyperspectral data using ATCOR-4 and FLAASH, and from in situ measurements of HCRF performed using the ASD FieldSpec 3 VNIR spectroradiometer. Note that several bands are excluded in the case of the white tarpaulin due to the saturation of the airborne hyperspectral data.

Table 5. Performance of ATCOR-4 and FLAASH over the white tarpaulin, grey tarpaulin, black tarpaulin, and artificial football field in the Valencia Anchor Station 2017 campaign, with respect to in situ measurements of HCRF between 350–1050 nm performed using the ASD FieldSpec 3 VNIR spectroradiometer.

	ATCOR-4			FLAASH		
Target	**RMSD**	**NRMSD (%)**	**Bias**	**RMSD**	**NRMSD (%)**	**Bias**
White tarpaulin	0.05	7.66	−0.03	0.07	10.53	−0.03
Grey tarpaulin	0.01	11.64	0.01	0.01	14.00	0.01
Black tarpaulin	0.01	15.85	0.00	0.02	55.05	0.02
Artificial football field	0.01	23.04	−0.01	0.01	21.03	−0.01

3.2. Characteristics of Airborne Hyperspectral and In Situ LAI, LCC, and CCC Data

Over the ESUs, the atmospherically corrected airborne hyperspectral reflectance data demonstrated typical spectral characteristics associated with deciduous broadleaf forest in the Wytham Woods 2018 and 2021 campaigns, with the chlorophyll and water absorption features clearly identifiable at blue, red, and shortwave-infrared wavelengths, as well as a clearly defined red-edge and near-infrared shoulder (Figure 5). Whilst reflectance appeared slightly higher in 2021 than in 2018, it is worth noting that a different number of ESUs were sampled (Section 2.4), so a direct comparison between the mean reflectance spectra is not possible. In the Valencia Anchor Station 2017 campaign, the strong contribution of the soil background to the reflectance signal was apparent, particularly in the visible and near-infrared region, where the chlorophyll absorption features and red-edge were less apparent, and in the shortwave-infrared region, where reflectance was substantially higher than in the Wytham Woods 2018 and 2021 campaigns (Figure 5).

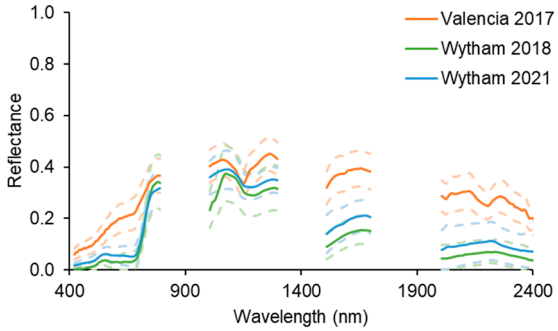

Figure 5. Mean (solid lines) and standard deviation (dashed lines) of observed airborne hyperspectral reflectance spectra over the considered ESUs in each campaign. Note that the excluded wavelengths correspond to noisy spectral regions dominated by water vapour absorption and dropouts (Section 2.3).

The sparse nature of the canopy in the Valencia Anchor Station 2017 campaign was equally evident in the in situ measurements of LAI, which were substantially lower and less variable (mean = 1.37, standard deviation = 0.68) than in the Wytham Woods 2018 and 2021 campaigns (mean = 4.35 and 4.22, standard deviation = 1.92 and 2.78) (Table 6). Differences in the in situ measurements of LCC were less distinct between the three campaigns (mean = 0.33 g m^{-2}, 0.31 g m^{-2}, and 0.28 g m^{-2}, standard deviation = 0.09 g m^{-2}, 0.16 g m^{-2}, and 0.19 g m^{-2}) (Table 6). However, as the product of LAI and LCC, substantially lower and less variable in situ CCC values were again observed in the Valencia Anchor Station 2017 campaign (mean = 0.41 g m^{-2}, standard deviation = 0.17 g m^{-2}) than in the Wytham Woods 2018 and 2021 campaigns (mean = 1.57 g m^{-2} and 1.60 g m^{-2}, standard deviation = 1.06 g m^{-2} and 1.43 g m^{-2}) (Table 6).

Table 6. Summary statistics associated with in situ LAI, LCC, and CCC measurements during each campaign.

Statistic	Valencia Anchor Station 2017			Wytham Woods 2018			Wytham Woods 2021		
	LAI	LCC ($g\ m^{-2}$)	CCC ($g\ m^{-2}$)	LAI	LCC ($g\ m^{-2}$)	CCC ($g\ m^{-2}$)	LAI	LCC ($g\ m^{-2}$)	CCC ($g\ m^{-2}$)
Minimum	0.41	0.21	0.15	0.00	0.00	0.00	0.00	0.00	0.00
Maximum	3.26	0.67	0.82	7.69	0.58	4.27	8.77	0.69	4.84
Mean	1.37	0.33	0.41	4.35	0.31	1.57	4.22	0.28	1.60
Standard deviation	0.68	0.09	0.17	1.92	0.16	1.06	2.78	0.19	1.43

3.3. Overall Performance of Turbid Medium and Hybrid Radiative Transfer Models

As hypothesised, SAIL-based LAI retrievals demonstrated moderate overall performance over the heterogeneous canopies investigated in this study (r^2 = 0.58, RMSD = 1.61, NRMSD = 50%, bias = 0.33). Notably, in the Valencia Anchor Station 2017 campaign, almost all retrievals were of LAI ~ 1, indicating a failure of SAIL to adequately simulate the canopy (Figure 6a). A similar, but less pronounced effect, was observed for the Wytham Woods 2018 and 2021 campaigns, where SAIL retrieved an LAI ~ 6 for a large number of ESUs where in situ LAI ranged from 2–9 (Figure 6a). Minimally vegetated ESUs (in situ LAI ~ 0) were substantially overestimated by SAIL (LAI ~ 4) in all cases (Figure 6a). When the hybrid radiative transfer models rowSAIL and INFORM were adopted, improved overall performance was observed (r^2 = 0.75, RMSD = 1.21, NRMSD = 38%, bias = −0.30), as was hypothesised, with a more realistic range of retrieved LAI values and increased correspondence with in situ LAI (Figure 6b).

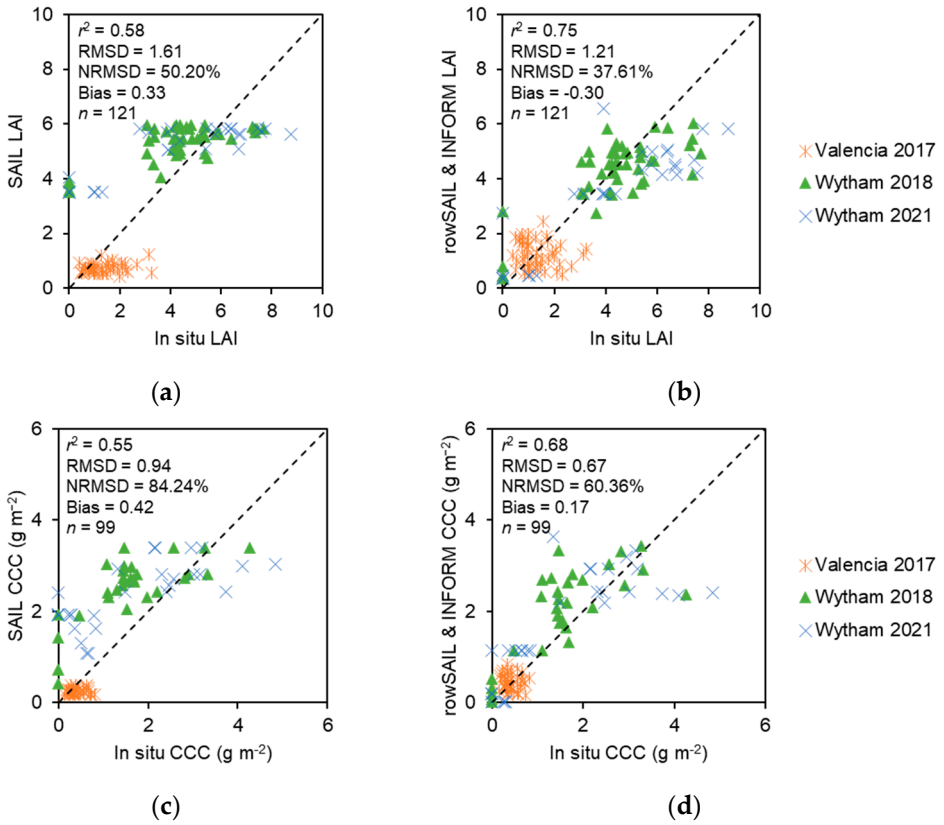

Figure 6. Validation of SAIL (**left**) and rowSAIL/INFORM (**right**) LAI (**a**,**b**) and CCC (**c**,**d**) retrievals against in situ measurements. The dashed line represents a 1:1 relationship.

We hypothesised that CCC would be subject to worse retrieval accuracy than LAI, because as the product of two terms, there are more opportunities for errors to propagate. Our results support this hypothesis, with lower r^2 and NRMSD values observed for CCC than for LAI retrievals (Figure 6c,d). In terms of the difference between the radiative transfer models, moderate performance was again provided by SAIL (r^2 = 0.55, RMSD = 0.94 g m^{-2}, NRMSD = 84%, bias = 0.42 g m^{-2}) (Figure 6c), but as with LAI, an improvement in overall performance was offered by rowSAIL and INFORM (r^2 = 0.68, RMSD = 0.67 g m^{-2}, NRMSD = 60%, bias = 0.17 g m^{-2}) (Figure 6d).

3.4. Performance of Turbid Medium and Hybrid Radiative Transfer Models by Campaign

As hypothesised, compared with the SAIL-based retrievals, rowSAIL and INFORM reduced the bias in LAI and CCC retrievals in all campaigns (Table 7). In both the Wytham Woods 2018 and 2021 campaigns, increased r^2 and decreased RMSD and NRMSD values were also associated with the INFORM-based retrievals (i.e., all performance statistics were improved with INFORM when compared to SAIL). This was not the case in the Valencia Anchor Station 2017 campaign, where the observed reduction in bias in rowSAIL CCC retrievals came at the expense of decreased precision, leading to a slightly increased RMSD (0.30 g m^{-2} as opposed to 0.27 g m^{-2}) and NRMSD (73% as opposed to 64%) when compared to the SAIL retrievals (Table 7). It is also worth noting that the Valencia Anchor Station 2017 campaign was characterised by low r^2 values for both variables and retrieval algorithms (Table 7). Given the RMSD and bias values achieved, this is likely a result of the very limited range in LAI and CCC values experienced at the site (Table 6), as previously noted by [37].

Table 7. Performance of SAIL and rowSAIL/INFORM LAI and CCC retrievals against in situ measurements, by campaign. The best performance statistic per campaign is shown in bold.

Model	Statistic	Valencia Anchor Station 2017		Wytham Woods 2018		Wytham Woods 2021	
		LAI	CCC (g m^{-2})	LAI	CCC (g m^{-2})	LAI	CCC (g m^{-2})
SAIL	r^2	**0.05**	0.00	0.55	0.56	0.73	0.53
	RMSD	0.92	**0.27**	1.74	1.12	2.15	1.27
	NRMSD (%)	67.05	**64.31**	40.05	71.59	50.87	79.15
	Bias	−0.64	−0.17	0.96	0.89	0.82	0.74
rowSAIL and INFORM	r^2	0.02	**0.01**	**0.64**	**0.58**	**0.76**	**0.62**
	RMSD	**0.88**	0.30	**1.16**	**0.82**	**1.64**	**0.87**
	NRMSD (%)	**64.44**	73.15	**26.70**	**52.08**	**38.85**	**54.23**
	Bias	**−0.13**	**0.03**	**−0.16**	**0.42**	**−0.78**	**0.10**

4. Discussion

4.1. Suitability of SAIL-Based Retrieval Algorithms over Heterogeneous Canopies

Accurate estimates of biophysical and biochemical variables such as LAI and CCC are essential in monitoring the condition of vegetation, and are key to modelling terrestrial productivity, carbon exchange, and the weather and climate systems [8,9,12]. Recent and upcoming spaceborne missions, including EnMAP, PRISMA, CHIME, and SBG, are set to provide an unprecedented stream of decametric hyperspectral observations that are ideally suited for the retrieval of these variables [69]. As a result, accurate and effective retrieval algorithms must be developed and evaluated.

In the context of climate change and an increasing global population, forests and agricultural environments are of particular importance, representing not only a vital carbon sink, but a source of food, resources, and ecosystem services [70–72]. Whilst several radiative transfer model-based retrieval algorithms have been developed for LAI and CCC retrieval from decametric hyperspectral observations (such as those provided by EnMAP, PRISMA, CHIME, and SBG), they have primarily focussed on cereal crops, making use of

SAIL to represent the canopy. Good retrieval accuracies have been reported in these studies for LAI (r^2 = 0.81–0.84, RMSD = 0.57–1.12) and CCC (r^2 = 0.72–0.88, RMSD = 0.21–0.59 g m^{-2}) [27–31], owing to the fact that SAIL can provide a good approximation of the dense, leafy, and homogeneous nature of the investigated canopies [35].

Despite the demonstrated utility of SAIL-based retrieval algorithms over cereal crops, data from recent and upcoming spaceborne decametric hyperspectral missions will also be applied for monitoring more heterogeneous environments such as forests and row-structured crops. At the canopy level, and as hypothesised based on previous work [25,34–36], our results suggest that SAIL is not well suited to LAI and CCC retrieval over such vegetation types. In a study focussed on retrieval from the Sentinel-2 Multispectral Instrument (MSI) over deciduous broadleaf forest, [35] demonstrated that the SAIL-based Sentinel-2 Level 2 Prototype Processor (SL2P) provided moderate performance for the retrieval of LAI and CCC. These results were subsequently confirmed over a wider range of forest types by [36,73]. Here, we show that the same conclusions apply to hyperspectral retrieval, not only over forest environments, but also over row-structured crops.

4.2. Utility of Hybrid Radiative Transfer Models over Heterogeneous Canopies

Our results demonstrate that by adopting hybrid radiative transfer models such as rowSAIL and INFORM, which enable factors such as crown transmittance, foliage clumping, and shadowing to be represented [17,20,39,41,42], reductions in bias can be achieved. The fact that the reduction in bias came at the cost of a slight decrease in precision for CCC retrievals in the Valencia Anchor Station 2017 campaign indicates there may be a trade-off between bias and precision when increasing the complexity of the adopted radiative transfer model (as also recently reported by [74] for forest LAI retrievals from Sentinel-2 MSI). Nevertheless, we suggest that addressing bias is of higher priority than addressing imprecision, since random errors will be reduced when synthesising over space and time in downstream applications [74].

Over forest environments such as Wytham Woods, our results are in agreement with those of [35], who achieved improved accuracy for INFORM-based retrievals of forest LAI (r^2 = 0.79, RMSD = 0.47, NRMSD = 13%, bias = −0.13) and CCC (r^2 = 0.69, RMSD = 0.52 g m^{-2}, NRMSD = 29%, bias = −0.08 g m^{-2}) from Sentinel-2 MSI when compared to SAIL-based LAI (r^2 = 0.54, RMSD = 1.55, NRMSD = 43%, bias = −1.38) and CCC (r^2 = 0.52, RMSD = 0.79 g m^{-2}, NRMSD = 45%, bias = −0.49) retrievals. Likewise, [74] applied an alternative hybrid radiative transfer model, 4SAIL2, for the retrieval of forest LAI from Sentinel-2 MSI, achieving similar improvements in accuracy (r^2 = 0.74, RMSD = 0.86, bias = −0.13) when compared to SAIL (r^2 = 0.67, RMSD = 0.91, bias = −0.38). Our results also reflect the findings of [41], who reported high accuracy when retrieving forest LAI from airborne hyperspectral data using INFORM (r^2 = 0.73, RMSD = 0.58). For row-structured crops, the improvement in retrieval accuracy achieved using rowSAIL over the Valencia Anchor Station reflects the work of [39,42], who applied the related rowMCRM radiative transfer model to account for the effects of vineyard structure.

Crucially, because hybrid radiative transfer models provide a more realistic description of the canopy than turbid medium radiative transfer models, but with a lower level of complexity than three-dimensional radiative transfer models, they remain relatively straightforward to invert. This is a key consideration, as the latter models require extensive parameterisation [20,41]. As a result, and due to hyperspectral data redundancy, the inversion of such models may be underdetermined; despite consisting of hundreds of spectral bands, the observations may contain too little information to solve for the number of unknowns. Offering an intermediate level of complexity, hybrid radiative transfer models effectively mitigate this issue.

4.3. Limitations and Perspectives for Future Work

Our study relied on airborne hyperspectral data, as the majority of our campaigns were conducted before spaceborne hyperspectral missions such as EnMAP and PRISMA

were operational (i.e., PRISMA was launched in 2019 and EnMAP was launched in 2022, whilst CHIME and SBG are scheduled for launch in the late 2020s). Although we made efforts to simulate the spatial and spectral characteristics of EnMAP, it is worth noting that the actual observational characteristics of these missions (such as the greater influence of atmospheric effects due to the longer atmospheric path length) could not be fully replicated. Given that uncertainties in atmospheric correction are likely to be higher for spaceborne (as opposed to airborne) observations, the retrieval accuracies reported in our study may be slightly overoptimistic (particularly in terms of precision), since errors in atmospheric correction will propagate through to LAI and CCC retrievals. Now that several spaceborne hyperspectral missions have been launched, future work should focus on confirming our findings with spaceborne observations. This will require dedicated and carefully planned campaigns, as the coverage of these missions is not systematic.

Biophysical and biochemical variables retrieved from hyperspectral data provide a rich source of information for deepening our understanding of vegetation physiology, and such information is vital for improving agricultural practices. By enabling the more accurate retrieval of LAI and CCC to be achieved over forests and row-structured crops, the results of our study are directly relevant to applications in precision agriculture. For instance, LAI is an indicator of biomass, and CCC is related to crop nitrogen content, providing valuable information about crop nutrient status [14,75,76]. Improved CCC retrievals can assist in the development of fertiliser treatment plans, enabling reduced environmental impact and maximised crop production. Likewise, more accurate LAI retrievals can be used as input to crop models to improve yield forecasting. Future work should assess the utility of hybrid radiative transfer models for the retrieval of additional variables, such as those related to vegetation water stress and of relevance for irrigation management (i.e., canopy water content) [77–79].

As users look to exploit spaceborne hyperspectral data for agricultural, forestry, and environmental management applications [69], freely available software tools for processing and analysing these data are likely to experience increased use. One such example is the EnMAP-Box [80], which provides a set of Agriculture Applications that include tools for the generation of look-up-tables, as well as look-up-table-based biophysical and biochemical variable retrieval [81]. In addition to SAIL, the EnMAP-Box Agriculture Applications already incorporate INFORM, meaning that our INFORM-based retrieval approach could easily be adopted by users of the toolbox for the retrieval of LAI and CCC over forest environments. As toolboxes such as the EnMAP-Box are developed and updated, other hybrid radiative transfer models such as rowSAIL should be incorporated to ensure utility in a wide range of environments. This will require clear guidance on model choice to be provided to users, to ensure appropriateness for the canopy of interest.

5. Conclusions

Although good retrieval accuracies have been reported over cereal crops for SAIL-based LAI and CCC retrieval algorithms developed in the context of missions such as EnMAP, PRISMA, CHIME, and SBG, few studies have investigated their performance over heterogeneous canopies. In this study, we explored hybrid radiative transfer models (rowSAIL and INFORM) to overcome the hypothesised limitations of SAIL. Our results demonstrate that over forests and row-structured crops, algorithms based on SAIL (which assumes horizontal homogeneity) provide moderate retrieval accuracy for LAI (RMSD = 0.92–2.15, NRMSD = 40–67%, bias = −0.64–0.96) and CCC (RMSD = 0.27–1.27 g m^{-2}, NRMSD = 64–84%, bias = −0.17–0.89 g m^{-2}). Hybrid radiative transfer models (which partition the canopy into geometric objects that are themselves treated as turbid media) could better represent heterogeneous vegetation, enabling reductions in bias to be achieved for LAI (RMSD = 0.88–1.64, NRMSD = 27–64%, bias = −0.78–−0.13) and CCC (RMSD = 0.30–0.87 g m^{-2}, NRMSD = 52–73%, bias = 0.03–0.42 g m^{-2}).

Based on our results, at the canopy level, we recommend that hybrid radiative transfer models such as rowSAIL and INFORM are further adopted for hyperspectral biophysical

and biochemical variable retrieval over heterogeneous vegetation. LAI and CCC are key inputs into models of terrestrial productivity, carbon exchange, and the weather and climate systems, so the associated reductions in systematic error achieved over these environments will facilitate better informed decisions in fields such as agriculture and forest management, as well as climate change mitigation and adaptation. As an unprecedented stream of hyperspectral observations becomes available from spaceborne missions, associated retrieval toolboxes should be developed and updated to incorporate such models. Clear guidance on model choice should also be provided to users, to ensure their appropriateness for the canopy of interest, as well as their utility in a wide range of downstream applications.

Author Contributions: Conceptualization, L.A.B.; methodology, L.A.B., A.L., C.L., I.B., D.C., G.L. and F.C.; software, L.A.B., H.M. and D.C.; validation, L.A.B., H.M., F.C. and J.D.; formal analysis, L.A.B., H.M., E.A., A.L., C.L., I.B., D.C., F.C. and J.P.-G.; investigation, L.A.B., H.M., A.M., F.D., J.A., E.L.-B., E.A., B.M., S.S.-R., M.C.-T., A.L., C.L., I.B., D.C., G.L., F.C., J.P.-G., R.M., M.S., O.W. and M.H.; resources, L.A.B., E.L.-B., B.M., S.S.-R., M.C.-T., A.L., C.L., I.B., D.C., G.L., F.C., A.H. and J.D.; data curation, L.A.B., H.M., E.A., B.M., S.S.-R., M.C.-T., A.L., C.L., I.B., D.C., G.L., F.C., J.P.-G. and A.H.; writing—original draft preparation, L.A.B.; writing—review and editing, L.A.B., H.M., A.M., F.D., J.A., E.L.-B., E.A., B.M., S.S.-R., M.C.-T., A.L., C.L., I.B., D.C., G.L., Q.X., F.C., J.P.-G., R.M., M.S., O.W., M.H., A.H., V.B., S.D. and J.D.; visualization, L.A.B., A.M. and J.P.-G.; supervision, L.A.B., E.L.-B., A.L., C.L., I.B., F.C., A.H. and J.D.; project administration, L.A.B., D.C., G.L., F.C., A.H., V.B., S.D. and J.D.; funding acquisition, L.A.B., F.C., A.H. and J.D. All authors have read and agreed to the published version of the manuscript.

Funding: This work was supported in part by the European Space Agency and European Commission through the Sentinel-3 Mission Performance Centre. This study has been undertaken using data from "Fiducial Reference Measurements for Vegetation" (FRM4VEG), which was funded by the European Commission and managed by the European Space Agency under the Copernicus programme, and "Fiducial Reference Measurements for Vegetation—Phase 2" (FRM4VEG—Phase 2), which was funded by the European Space Agency. This activity was carried out under the Living Planet Fellowship, a programme of and funded by the European Space Agency. The view expressed in this publication can in no way be taken to reflect the official opinion of the European Space Agency. This work was supported by MetEOC-4. The project 19ENV07 MetEOC-4 has received funding from the EMPIR programme co-financed by the Participating States and from the European Union's Horizon 2020 research and innovation programme.

Data Availability Statement: Dataset available upon request from the authors.

Acknowledgments: The authors extend their gratitude to Nigel Fisher and the University of Oxford for facilitating access to Wytham Woods, in addition to Jaan Praks and Clement Atzberger for providing copies of rowMCRM and INFORM. The authors are also grateful to Pilar Campíns-Falcó, Domingo Catalan, Amparo Coll Pajaron, María Amparo Gilabert, Aida Vicente, Nadine Gobron, Christian Lanconelli, Olivier Morgan, Domingo Iglesias, and Beatriz Fuster for their assistance in campaign planning and execution. The authors gratefully acknowledge the Natural Environment Research Council Airborne Research Facility and Data Analysis Node for the acquisition and processing of airborne hyperspectral data, and the Field Spectroscopy Facility for loan of the tarpaulins, provision of guidance, and cleaning and calibration of the Spectralon panel.

Conflicts of Interest: Author Gary Llewellyn is employed by 2Excel Geo and author Rosalinda Morrone is employed by Starion. The authors declare no conflicts of interest.

References

1. Guanter, L.; Kaufmann, H.; Segl, K.; Foerster, S.; Rogass, C.; Chabrillat, S.; Kuester, T.; Hollstein, A.; Rossner, G.; Chlebek, C.; et al. The EnMAP Spaceborne Imaging Spectroscopy Mission for Earth Observation. *Remote Sens.* **2015**, *7*, 8830–8857. [CrossRef]
2. Cogliati, S.; Sarti, F.; Chiarantini, L.; Cosi, M.; Lorusso, R.; Lopinto, E.; Miglietta, F.; Genesio, L.; Guanter, L.; Damm, A.; et al. The PRISMA Imaging Spectroscopy Mission: Overview and First Performance Analysis. *Remote Sens. Environ.* **2021**, *262*, 112499. [CrossRef]
3. Nieke, J.; Rast, M. Towards the Copernicus Hyperspectral Imaging Mission For The Environment (CHIME). In Proceedings of the 2018 IEEE International Geoscience and Remote Sensing Symposium, Valencia, Spain, 22–27 July 2018; Institute of Electrical and Electronics Engineers: Valencia, Spain, 2018; pp. 157–159.

4. Stavros, E.N.; Chrone, J.; Cawse-Nicholson, K.; Freeman, A.; Glenn, N.F.; Guild, L.; Kokaly, R.; Lee, C.; Luvall, J.; Pavlick, R.; et al. Designing an Observing System to Study the Surface Biology and Geology (SBG) of the Earth in the 2020s. *J. Geophys. Res. Biogeosci.* **2023**, *128*, e2021JG006471. [CrossRef]
5. Barnsley, M.J.; Settle, J.J.; Cutter, M.A.; Lobb, D.R.; Teston, F. The PROBA/CHRIS Mission: A Low-Cost Smallsat for Hyperspectral Multiangle Observations of the Earth Surface and Atmosphere. *IEEE Trans. Geosci. Remote Sens.* **2004**, *42*, 1512–1520. [CrossRef]
6. Chen, J.M.; Black, T.A. Measuring Leaf Area Index of Plant Canopies with Branch Architecture. *Agric. For. Meteorol.* **1991**, *57*, 1–12. [CrossRef]
7. Gitelson, A.A.; Viña, A.; Ciganda, V.; Rundquist, D.C.; Arkebauer, T.J. Remote Estimation of Canopy Chlorophyll Content in Crops. *Geophys. Res. Lett.* **2005**, *32*, 1–4. [CrossRef]
8. Richardson, A.D.; Keenan, T.F.; Migliavacca, M.; Ryu, Y.; Sonnentag, O.; Toomey, M. Climate Change, Phenology, and Phenological Control of Vegetation Feedbacks to the Climate System. *Agric. For. Meteorol.* **2013**, *169*, 156–173. [CrossRef]
9. Sellers, P.J.; Dickinson, R.E.; Randall, D.A.; Betts, A.K.; Hall, F.G.; Berry, J.A.; Collatz, G.J.; Denning, A.S.; Mooney, H.A.; Nobre, C.A.; et al. Modeling the Exchanges of Energy, Water, and Carbon Between Continents and the Atmosphere. *Science* **1997**, *275*, 502–509. [CrossRef]
10. Clevers, J.G.P.W.; Gitelson, A.A. Remote Estimation of Crop and Grass Chlorophyll and Nitrogen Content Using Red-Edge Bands on Sentinel-2 and -3. *Int. J. Appl. Earth Obs. Geoinf.* **2013**, *23*, 344–351. [CrossRef]
11. Lichtenthaler, H.K.; Wenzel, O.; Buschmann, C.; Gitelson, A. Plant Stress Detection by Reflectance and Fluorescence. *Ann. N. Y. Acad. Sci.* **1998**, *851*, 271–285. [CrossRef]
12. Ogutu, B.O.; Dash, J.; Dawson, T.P. Developing a Diagnostic Model for Estimating Terrestrial Vegetation Gross Primary Productivity Using the Photosynthetic Quantum Yield and Earth Observation Data. *Glob. Chang. Biol.* **2013**, *19*, 2878–2892. [CrossRef]
13. Verrelst, J.; Camps-Valls, G.; Muñoz-Marí, J.; Rivera, J.P.; Veroustraete, F.; Clevers, J.G.P.W.; Moreno, J. Optical Remote Sensing and the Retrieval of Terrestrial Vegetation Bio-Geophysical Properties—A Review. *ISPRS J. Photogramm. Remote Sens.* **2015**, *108*, 273–290. [CrossRef]
14. Verrelst, J.; Malenovský, Z.; Van der Tol, C.; Camps-Valls, G.; Gastellu-Etchegorry, J.-P.; Lewis, P.; North, P.; Moreno, J. Quantifying Vegetation Biophysical Variables from Imaging Spectroscopy Data: A Review on Retrieval Methods. *Surv. Geophys.* **2019**, *40*, 589–629. [CrossRef]
15. Colombo, R.; Bellingeri, D.; Fasolini, D.; Marino, C.M. Retrieval of Leaf Area Index in Different Vegetation Types Using High Resolution Satellite Data. *Remote Sens. Environ.* **2003**, *86*, 120–131. [CrossRef]
16. Dash, J.; Ogutu, B.O. Recent Advances in Space-Borne Optical Remote Sensing Systems for Monitoring Global Terrestrial Ecosystems. *Prog. Phys. Geogr.* **2016**, *40*, 322–351. [CrossRef]
17. Dorigo, W.A.; Zurita-Milla, R.; de Wit, A.J.W.; Brazile, J.; Singh, R.; Schaepman, M.E. A Review on Reflective Remote Sensing and Data Assimilation Techniques for Enhanced Agroecosystem Modeling. *Int. J. Appl. Earth Obs. Geoinf.* **2007**, *9*, 165–193. [CrossRef]
18. Houborg, R.; Soegaard, H.; Boegh, E. Combining Vegetation Index and Model Inversion Methods for the Extraction of Key Vegetation Biophysical Parameters Using Terra and Aqua MODIS Reflectance Data. *Remote Sens. Environ.* **2007**, *106*, 39–58. [CrossRef]
19. Liang, S. Recent Developments in Estimating Land Surface Biogeophysical Variables from Optical Remote Sensing. *Prog. Phys. Geogr.* **2007**, *31*, 501–516. [CrossRef]
20. Roberts, G. A Review of the Application of BRDF Models to Infer Land Cover Parameters at Regional and Global Scales. *Prog. Phys. Geogr.* **2001**, *25*, 483–511. [CrossRef]
21. Atzberger, C.; Richter, K.; Vuolo, F.; Darvishzadeh, R.; Schlerf, M. Why Confining to Vegetation Indices? Exploiting the Potential of Improved Spectral Observations Using Radiative Transfer Models. *Remote Sens. Agric. Ecosyst. Hydrol. XIII* **2011**, *8174*, 81740Q. [CrossRef]
22. Camacho, F.; Fuster, B.; Li, W.; Weiss, M.; Ganguly, S.; Lacaze, R.; Baret, F. Crop Specific Algorithms Trained over Ground Measurements Provide the Best Performance for GAI and FAPAR Estimates from Landsat-8 Observations. *Remote Sens. Environ.* **2021**, *260*, 112453. [CrossRef]
23. Bacour, C.; Baret, F.; Béal, D.; Weiss, M.; Pavageau, K. Neural Network Estimation of LAI, FAPAR, FCover and LAIxCab, from Top of Canopy MERIS Reflectance Data: Principles and Validation. *Remote Sens. Environ.* **2006**, *105*, 313–325. [CrossRef]
24. Kimes, D.S.; Knyazikhin, Y.; Privette, J.L.; Abuelgasim, A.A.; Gao, F. Inversion Methods for Physically-based Models. *Remote Sens. Rev.* **2000**, *18*, 381–439. [CrossRef]
25. Verger, A.; Baret, F.; Camacho, F. Optimal Modalities for Radiative Transfer-Neural Network Estimation of Canopy Biophysical Characteristics: Evaluation over an Agricultural Area with CHRIS/PROBA Observations. *Remote Sens. Environ.* **2011**, *115*, 415–426. [CrossRef]
26. Weiss, M.; Baret, F.; Myneni, R.B.; Pragnère, A.; Knyazikhin, Y. Investigation of a Model Inversion Technique to Estimate Canopy Biophysical Variables from Spectral and Directional Reflectance Data. *Agronomie* **2000**, *20*, 3–22. [CrossRef]
27. Wocher, M.; Berger, K.; Danner, M.; Mauser, W.; Hank, T. RTM-Based Dynamic Absorption Integrals for the Retrieval of Biochemical Vegetation Traits. *Int. J. Appl. Earth Obs. Geoinf.* **2020**, *93*, 102219. [CrossRef]

28. Danner, M.; Berger, K.; Wocher, M.; Mauser, W.; Hank, T. Efficient RTM-Based Training of Machine Learning Regression Algorithms to Quantify Biophysical & Biochemical Traits of Agricultural Crops. *ISPRS J. Photogramm. Remote Sens.* **2021**, *173*, 278–296. [CrossRef]
29. Tagliabue, G.; Boschetti, M.; Bramati, G.; Candiani, G.; Colombo, R.; Nutini, F.; Pompilio, L.; Rivera-Caicedo, J.P.; Rossi, M.; Rossini, M.; et al. Hybrid Retrieval of Crop Traits from Multi-Temporal PRISMA Hyperspectral Imagery. *ISPRS J. Photogramm. Remote Sens.* **2022**, *187*, 362–377. [CrossRef]
30. Pascual-Venteo, A.B.; Portalés, E.; Berger, K.; Tagliabue, G.; Garcia, J.L.; Pérez-Suay, A.; Rivera-Caicedo, J.P.; Verrelst, J. Prototyping Crop Traits Retrieval Models for CHIME: Dimensionality Reduction Strategies Applied to PRISMA Data. *Remote Sens.* **2022**, *14*, 2448. [CrossRef]
31. Candiani, G.; Tagliabue, G.; Panigada, C.; Verrelst, J.; Picchi, V.; Rivera Caicedo, J.P.; Boschetti, M. Evaluation of Hybrid Models to Estimate Chlorophyll and Nitrogen Content of Maize Crops in the Framework of the Future CHIME Mission. *Remote Sens.* **2022**, *14*, 1792. [CrossRef]
32. Verhoef, W. Light Scattering by Leaf Layers with Application to Canopy Reflectance Modeling: The SAIL Model. *Remote Sens. Environ.* **1984**, *16*, 125–141. [CrossRef]
33. Verhoef, W.; Jia, L.; Xiao, Q.; Su, Z. Unified Optical-Thermal Four-Stream Radiative Transfer Theory for Homogeneous Vegetation Canopies. *IEEE Trans. Geosci. Remote Sens.* **2007**, *45*, 1808–1822. [CrossRef]
34. Richter, K.; Atzberger, C.; Vuolo, F.; Weihs, P.; D'Urso, G. Experimental Assessment of the Sentinel-2 Band Setting for RTM-Based LAI Retrieval of Sugar Beet and Maize. *Can. J. Remote Sens.* **2009**, *35*, 230–247. [CrossRef]
35. Brown, L.A.; Ogutu, B.O.; Dash, J. Estimating Forest Leaf Area Index and Canopy Chlorophyll Content with Sentinel-2: An Evaluation of Two Hybrid Retrieval Algorithms. *Remote Sens.* **2019**, *11*, 1752. [CrossRef]
36. Brown, L.A.; Fernandes, R.; Djamai, N.; Meier, C.; Gobron, N.; Morris, H.; Canisius, F.; Bai, G.; Lerebourg, C.; Lanconelli, C.; et al. Validation of Baseline and Modified Sentinel-2 Level 2 Prototype Processor Leaf Area Index Retrievals over the United States. *ISPRS J. Photogramm. Remote Sens.* **2021**, *175*, 71–87. [CrossRef]
37. Brown, L.A.; Dash, J.; Lidon, A.L.; Lopez-Baeza, E.; Dransfeld, S. Synergetic Exploitation of the Sentinel-2 Missions for Validating the Sentinel-3 Ocean and Land Color Instrument Terrestrial Chlorophyll Index Over a Vineyard Dominated Mediterranean Environment. *IEEE J. Sel. Top. Appl. Earth Obs. Remote Sens.* **2019**, *12*, 2244–2251. [CrossRef]
38. Yuan, H.; Ma, R.; Atzberger, C.; Li, F.; Loiselle, S.; Luo, J. Estimating Forest FAPAR from Multispectral Landsat-8 Data Using the Invertible Forest Reflectance Model INFORM. *Remote Sens.* **2015**, *7*, 7425–7446. [CrossRef]
39. Meggio, F.; Zarco-Tejada, P.J.; Miller, J.R.; Martín, P.; González, M.R.; Berjón, A. Row Orientation and Viewing Geometry Effects on Row-Structured Vine Crops for Chlorophyll Content Estimation. *Can. J. Remote Sens.* **2008**, *34*, 220–234. [CrossRef]
40. Darvishzadeh, R.; Skidmore, A.; Abdullah, H.; Cherenet, E.; Ali, A.; Wang, T.; Nieuwenhuis, W.; Heurich, M.; Vrieling, A.; O'Connor, B.; et al. Mapping Leaf Chlorophyll Content from Sentinel-2 and RapidEye Data in Spruce Stands Using the Invertible Forest Reflectance Model. *Int. J. Appl. Earth Obs. Geoinf.* **2019**, *79*, 58–70. [CrossRef]
41. Schlerf, M.; Atzberger, C. Inversion of a Forest Reflectance Model to Estimate Structural Canopy Variables from Hyperspectral Remote Sensing Data. *Remote Sens. Environ.* **2006**, *100*, 281–294. [CrossRef]
42. Zarco-Tejada, P.J.; Berjón, A.; López-Lozano, R.; Miller, J.R.; Martín, P.; Cachorro, V.; González, M.R.; De Frutos, A. Assessing Vineyard Condition with Hyperspectral Indices: Leaf and Canopy Reflectance Simulation in a Row-Structured Discontinuous Canopy. *Remote Sens. Environ.* **2005**, *99*, 271–287. [CrossRef]
43. Lopez-Baeza, E.; Antolin, C.; Belda, F.; Carbo, E.; Coll, A.; Estrela, T.; Fernández, R.; Fidalgo, A.; Gabaldo, O.; Juglea, S.; et al. SMOS Land Validation Activities at the Valencia Anchor Station. In Proceedings of the XV Congreso de la Asociación Española de Teledetección, Madrid, Spain, 22–24 October 2013; Instituto Nacional de Tecnica Aeroespacia: Torrejón de Ardoz, Spain, 2013.
44. Specim AisaFENIX Hyperspectral Sensor. Available online: http://www.specim.fi/hyperspectral-remote-sensing/ (accessed on 24 August 2018).
45. Chapman, J.W.; Thompson, D.R.; Helmlinger, M.C.; Bue, B.D.; Green, R.O.; Eastwood, M.L.; Geier, S.; Olson-Duvall, W.; Lundeen, S.R. Spectral and Radiometric Calibration of the Next Generation Airborne Visible Infrared Spectrometer (AVIRIS-NG). *Remote Sens.* **2019**, *11*, 2129. [CrossRef]
46. Hueni, A.; Eastwood, M.; Meiller, C.; Werfeli, M.; Kuehnle, H.; Green, R.; Schaepman, M.; Nieke, J.; Rast, M. Joint NASA and ESA Imaging Spectrometer Airborne Campaign to Support SBG and CHIME. In Proceedings of the AGU Fall Meeting 2021, New Orleans, LA, USA, 13–17 December 2021; American Geophysical Union: New Orleans, LA, USA, 2021; p. GC13A–06.
47. Thompson, D.R.; Natraj, V.; Green, R.O.; Helmlinger, M.C.; Gao, B.-C.; Eastwood, M.L. Optimal Estimation for Imaging Spectrometer Atmospheric Correction. *Remote Sens. Environ.* **2018**, *216*, 355–373. [CrossRef]
48. Berk, A.; Anderson, G.P.; Acharya, P.K.; Bernstein, L.S.; Muratov, L.; Lee, J.; Fox, M.J.; Adler-Golden, S.M.; Chetwynd, J.H., Jr.; Hoke, M.L.; et al. MODTRAN5: A Reformulated Atmospheric Band Model with Auxiliary Species and Practical Multiple Scattering Options. In Proceedings of the 2004 SPIE International Symposium on Defense and Security, Kissimmee, FL, USA, 12–16 April 2004; Shen, S.S., Lewis, P.E., Eds.; Society of Photo-Optical Instrumentation Engineers: Orlando, FL, USA, 2004.
49. Wilson, R.T.; Milton, E.J.; Nield, J.M. Are Visibility-Derived AOT Estimates Suitable for Parameterizing Satellite Data Atmospheric Correction Algorithms? *Int. J. Remote Sens.* **2015**, *36*, 1675–1688. [CrossRef]
50. Kennedy, R.E.; Cohen, W.B.; Takao, G. Empirical Methods to Compensate for a View-Angle-Dependent Brightness Gradient in AVIRIS Imagery. *Remote Sens. Environ.* **1997**, *62*, 277–291. [CrossRef]

51. Warren, M.A.; Taylor, B.H.; Grant, M.G.; Shutler, J.D. Data Processing of Remotely Sensed Airborne Hyperspectral Data Using the Airborne Processing Library (APL): Geocorrection Algorithm Descriptions and Spatial Accuracy Assessment. *Comput. Geosci.* **2014**, *64*, 24–34. [CrossRef]
52. Atzberger, C. Development of an Invertible Forest Reflectance Model the INFORM-Model. In Proceedings of the 20th EARSeL Symposium, Dresden, Germany, 14–16 June 2000; Buchroithner, Ed.; European Association of Remote Sensing Laboratories: Dresden, Germany, 2000; pp. 39–44.
53. Adams, J.; Lewis, P.; Disney, M. Decoupling Canopy Structure and Leaf Biochemistry: Testing the Utility of Directional Area Scattering Factor (DASF). *Remote Sens.* **2018**, *10*, 1911. [CrossRef]
54. Ma, X.; Wang, T.; Lu, L. A Refined Four-Stream Radiative Transfer Model for Row-Planted Crops. *Remote Sens.* **2020**, *12*, 1290. [CrossRef]
55. Huang, H. Accelerated RAPID Model Using Heterogeneous Porous Objects. *Remote Sens.* **2018**, *10*, 1264. [CrossRef]
56. Feret, J.-B.; François, C.; Asner, G.P.; Gitelson, A.A.; Martin, R.E.; Bidel, L.P.R.; Ustin, S.L.; le Maire, G.; Jacquemoud, S. PROSPECT-4 and 5: Advances in the Leaf Optical Properties Model Separating Photosynthetic Pigments. *Remote Sens. Environ.* **2008**, *112*, 3030–3043. [CrossRef]
57. Jacquemoud, S.; Baret, F. PROSPECT: A Model of Leaf Optical Properties Spectra. *Remote Sens. Environ.* **1990**, *34*, 75–91. [CrossRef]
58. Baldridge, A.M.; Hook, S.J.; Grove, C.I.; Rivera, G. The ASTER Spectral Library Version 2.0. *Remote Sens. Environ.* **2009**, *113*, 711–715. [CrossRef]
59. Richter, K.; Hank, T.B.; Vuolo, F.; Mauser, W.; D'Urso, G. Optimal Exploitation of the Sentinel-2 Spectral Capabilities for Crop Leaf Area Index Mapping. *Remote Sens.* **2012**, *4*, 561–582. [CrossRef]
60. Rivera, J.; Verrelst, J.; Leonenko, G.; Moreno, J. Multiple Cost Functions and Regularization Options for Improved Retrieval of Leaf Chlorophyll Content and LAI through Inversion of the PROSAIL Model. *Remote Sens.* **2013**, *5*, 3280–3304. [CrossRef]
61. Verrelst, J.; Rivera, J.P.; Leonenko, G.; Alonso, L.; Moreno, J. Optimizing LUT-Based RTM Inversion for Semiautomatic Mapping of Crop Biophysical Parameters from Sentinel-2 and -3 Data: Role of Cost Functions. *IEEE Trans. Geosci. Remote Sens.* **2014**, *52*, 257–269. [CrossRef]
62. Darvishzadeh, R.; Skidmore, A.; Schlerf, M.; Atzberger, C. Inversion of a Radiative Transfer Model for Estimating Vegetation LAI and Chlorophyll in a Heterogeneous Grassland. *Remote Sens. Environ.* **2008**, *112*, 2592–2604. [CrossRef]
63. Brown, L.A.; Camacho, F.; García-Santos, V.; Origo, N.; Fuster, B.; Morris, H.; Pastor-Guzman, J.; Sánchez-Zapero, J.; Morrone, R.; Ryder, J.; et al. Fiducial Reference Measurements for Vegetation Bio-Geophysical Variables: An End-to-End Uncertainty Evaluation Framework. *Remote Sens.* **2021**, *13*, 3194. [CrossRef]
64. Fernandes, R.; Plummer, S.; Nightingale, J.; Baret, F.; Camacho, F.; Fang, H.; Garrigues, S.; Gobron, N.; Lang, M.; Lacaze, R.; et al. Global Leaf Area Index Product Validation Good Practices. In *Best Practice for Satellite-Derived Land Product Validation*; Fernandes, R., Plummer, S., Nightingale, J., Eds.; Land Product Validation Subgroup (Committee on Earth Observation Satellites Working Group on Calibration and Validation): Sioux Falls, SD, USA, 2014.
65. Brown, L.A.; Morris, H.; Leblanc, S.; Bai, G.; Lanconelli, C.; Gobron, N.; Meier, C.; Dash, J. HemiPy: A Python Module for Automated Estimation of Forest Biophysical Variables and Uncertainties from Digital Hemispherical Photographs. *Methods Ecol. Evol.* **2023**, *14*, 2329–2340. [CrossRef]
66. Weiss, M.; Baret, F. *CAN-EYE V6.4.91 User Manual*; Institut National de la Recherche Agronomique: Avignon, France, 2017.
67. Brown, L.A.; Williams, O.; Dash, J. Calibration and Characterisation of Four Chlorophyll Meters and Transmittance Spectroscopy for Non-Destructive Estimation of Forest Leaf Chlorophyll Concentration. *Agric. For. Meteorol.* **2022**, *323*, 109059. [CrossRef]
68. Vuolo, F.; Dash, J.; Curran, P.J.; Lajas, D.; Kwiatkowska, E. Methodologies and Uncertainties in the Use of the Terrestrial Chlorophyll Index for the Sentinel-3 Mission. *Remote Sens.* **2012**, *4*, 1112–1133. [CrossRef]
69. Hank, T.B.; Berger, K.; Bach, H.; Clevers, J.G.P.W.; Gitelson, A.; Zarco-Tejada, P.; Mauser, W. Spaceborne Imaging Spectroscopy for Sustainable Agriculture: Contributions and Challenges. *Surv. Geophys.* **2019**, *40*, 515–551. [CrossRef]
70. Foley, J.A.; Ramankutty, N.; Brauman, K.A.; Cassidy, E.S.; Gerber, J.S.; Johnston, M.; Mueller, N.D.; O'Connell, C.; Ray, D.K.; West, P.C.; et al. Solutions for a Cultivated Planet. *Nature* **2011**, *478*, 337–342. [CrossRef]
71. Godfray, H.C.J.; Beddington, J.R.; Crute, I.R.; Haddad, L.; Lawrence, D.; Muir, J.F.; Pretty, J.; Robinson, S.; Thomas, S.M.; Toulmin, C. Food Security: The Challenge of Feeding 9 Billion People. *Science* **2010**, *327*, 812–818. [CrossRef]
72. Beer, C.; Reichstein, M.; Tomelleri, E.; Ciais, P.; Jung, M.; Carvalhais, N.; Rodenbeck, C.; Arain, M.A.; Baldocchi, D.; Bonan, G.B.; et al. Terrestrial Gross Carbon Dioxide Uptake: Global Distribution and Covariation with Climate. *Science* **2010**, *329*, 834–838. [CrossRef]
73. Fernandes, R.; Brown, L.; Canisius, F.; Dash, J.; He, L.; Hong, G.; Huang, L.; Le, N.Q.; MacDougall, C.; Meier, C.; et al. Validation of Simplified Level 2 Prototype Processor Sentinel-2 Fraction of Canopy Cover, Fraction of Absorbed Photosynthetically Active Radiation and Leaf Area Index Products over North American Forests. *Remote Sens. Environ.* **2023**, *293*, 113600. [CrossRef]
74. Fernandes, R.; Djamai, N.; Harvey, K.; Hong, G.; MacDougall, C.; Shah, H.; Sun, L. Evidence of a Bias-Variance Trade off When Correcting for Bias in Sentinel 2 Forest LAI Retrievals Using Radiative Transfer Models. *Remote Sens. Environ.* **2024**, *305*, 114060. [CrossRef]
75. Li, W.; Weiss, M.; Jay, S.; Wei, S.; Zhao, N.; Comar, A.; Lopez-Lozano, R.; De Solan, B.; Yu, Q.; Wu, W.; et al. Daily Monitoring of Effective Green Area Index and Vegetation Chlorophyll Content from Continuous Acquisitions of a Multi-Band Spectrometer over Winter Wheat. *Remote Sens. Environ.* **2024**, *300*, 113883. [CrossRef]

76. Berger, K.; Verrelst, J.; Féret, J.-B.; Wang, Z.; Wocher, M.; Strathmann, M.; Danner, M.; Mauser, W.; Hank, T. Crop Nitrogen Monitoring: Recent Progress and Principal Developments in the Context of Imaging Spectroscopy Missions. *Remote Sens. Environ.* **2020**, *242*, 111758. [CrossRef]
77. Colombo, R.; Meroni, M.; Marchesi, A.; Busetto, L.; Rossini, M.; Giardino, C.; Panigda, C. Estimation of Leaf and Canopy Water Content in Poplar Plantations by Means of Hyperspectral Indices and Inverse Modeling. *Remote Sens. Environ.* **2008**, *112*, 1820–1834. [CrossRef]
78. Clevers, J.G.P.W.; Kooistra, L.; Schaepman, M.E. Estimating Canopy Water Content Using Hyperspectral Remote Sensing Data. *Int. J. Appl. Earth Obs. Geoinf.* **2010**, *12*, 119–125. [CrossRef]
79. Rollin, E.M.; Milton, E.J. Processing of High Spectral Resolution Reflectance Data for the Retrieval of Canopy Water Content Information. *Remote Sens. Environ.* **1998**, *65*, 86–92. [CrossRef]
80. Jakimow, B.; Janz, A.; Thiel, F.; Okujeni, A.; Hostert, P.; van der Linden, S. EnMAP-Box: Imaging Spectroscopy in QGIS. *SoftwareX* **2023**, *23*, 101507. [CrossRef]
81. Hank, T.; Berger, K.; Wocher, M.; Danner, M.; Mauser, W. Introducing the Potential of the EnMAP-Box for Agricultural Applications Using DESIS and PRISMA Data. In Proceedings of the 2021 IEEE International Geoscience and Remote Sensing Symposium, Brussels, Belgium, 11–16 July 2021; Institute of Electrical and Electronics Engineers: Brussels, Belgium, 2021; pp. 467–470.